



LAWRENCE
LIVERMORE
NATIONAL
LABORATORY

Fabrication of flexible, aligned carbon nanotube/polymer composite membranes by in-situ polymerization

S. Kim, F. Fornasiero, H. G. Park, J. B. In, E. Meshot, G. Giraldo, M. Stadermann, M. Fireman, J. Shan, C. P. Grigoropoulos, O. Bakajin

July 18, 2013

Journal of Membrane Science

Disclaimer

This document was prepared as an account of work sponsored by an agency of the United States government. Neither the United States government nor Lawrence Livermore National Security, LLC, nor any of their employees makes any warranty, expressed or implied, or assumes any legal liability or responsibility for the accuracy, completeness, or usefulness of any information, apparatus, product, or process disclosed, or represents that its use would not infringe privately owned rights. Reference herein to any specific commercial product, process, or service by trade name, trademark, manufacturer, or otherwise does not necessarily constitute or imply its endorsement, recommendation, or favoring by the United States government or Lawrence Livermore National Security, LLC. The views and opinions of authors expressed herein do not necessarily state or reflect those of the United States government or Lawrence Livermore National Security, LLC, and shall not be used for advertising or product endorsement purposes.

Fabrication of flexible, aligned carbon nanotube/polymer composite membranes by in-situ polymerization

Sangil Kim^{1*}, Francesco Fornasiero¹, HyungGyu Park², Jung Bin In³, Eric Meshot¹, Gabriel Giraldo⁴, Michael Stadermann¹, Micha Fireman⁵, Jerry Shan⁴, Costas P. Grigoropoulos³, and Olgica Bakajin⁵

¹Lawrence Livermore National Laboratory, Livermore CA 94550

²Department of Mechanical and Process Engineering, ETH Zurich, Zurich CH-8092, Switzerland

³Department of Mechanical Engineering, University of California Berkeley, Berkeley, CA 94720

⁴Department of Mechanical and Aerospace Engineering, Rutgers University, NJ 08854

⁵Porifera Inc., Hayward, CA 94545

*Corresponding author: kim55@llnl.gov

Abstract

Vertically aligned (VA) carbon nanotubes (CNTs) have shown orders of magnitude enhancement for gas and liquid flow compared to conventional mass transport theories. Flexible, large surface-area VACNT membranes may provide a cost-efficient solution to various separation processes such as water purification and gas separation. However, all the VACNT membranes produced so far suffer from rather small membrane area, long fabrication process, poor mechanical stability, local agglomeration of CNTs, and low CNT packing density. Here, we present flexible, VACNT/polymer composite membranes having relatively densely packed CNTs as the only mass transport paths. In order to prevent CNT condensation that could disturb CNT orientation during liquid phase processing, we developed a novel in-situ bulk polymerization method to prepare VACNT/polymer composite films. A VACNT array was infiltrated with styrene monomer with a certain amount of polystyrene-polybutadiene (PS-PB) copolymer that acts as a plasticizer. Indeed, micro-indentation measurements confirmed that the addition PS-b-PB copolymer into the matrix improved the elongation at break of the CNT/PS composite film. SEM images showed that well aligned CNTs were embedded in a high-density polymer matrix free of any macroscopic voids or structural defects. Measured fluid rates and selectivity for gas and liquid mixtures are consistent with CNT membranes produced in different methods. These CNTs/polymer composite membranes showed high gas and water permeability comparable to the other VACNT composite membranes, potentially enabling applications that may require membranes with high flux, flexibility and durability.

1. Introduction

Exceptional electrical, thermal, mechanical, and mass transport properties of CNTs¹⁻⁷ make the CNTs a promising nanoporous material for applications in membrane separation. One-dimensional graphitic nanochannel structure of CNT's is of particular interest as a building block for the next generation membranes.^{5,6,8-12} Exciting predictions from molecular dynamics simulations have motivated fabrication of CNT membrane platforms to develop new membrane materials with extremely large gas or water permeation. Hummer *et al.* have found that water molecules could transport in a single-file configuration through narrow CNTs at ultrahigh rates due to molecular ordering and tight hydrogen bonding under extreme graphitic nanoconfinement.¹³ Atomistic simulation studies by Sholl *et al.* have also predicted unprecedentedly large gas permeation and selectivity of CNTs due to their atomically smooth wall and preferential gas-wall interactions.¹⁴

Several research groups have experimentally verified predictions of MD simulations by employing CNT membranes fabricated by different methods. Hinds *et al.* first fabricated multi walled VACNT (MWCNT) membranes with an inner core diameter of *ca.* 6 nm embedded in a rigid polystyrene matrix.⁵ They demonstrated that liquid transport through the MWCNT membrane was several orders of magnitude faster than predictions from classical hydrodynamics theory.¹⁵ Holt *et al.* have adopted a micro fabrication method⁶ to produce membranes in which 1.6-nm-wide double-walled CNTs (DWNT) serve as only through-pores spanning a silicon nitride matrix deposited by chemical vapor deposition (CVD). Reported values of liquid and gas flows in DWNTs were several orders of magnitude larger than predicted by conventional hydrodynamics and Knudsen diffusion model, respectively. Miao *et al.* have used a matrix-free approach to fabricate CNT membranes:¹¹ capillary forces during solvent wetting and evaporation from as-grown CNT arrays produced small-size CNT mats with densities a few orders of magnitude higher than in other CNT membranes. Kim *et al.* developed a scalable, fabrication method,⁹ in which a preferential vertical alignment of single-walled CNTs (SWNTs) was achieved during filtration of a SWNT dispersion through a porous membrane, followed by sealing of the inter-SWNT spacing with spin-coated polysulfone. The prepared SWNT membrane showed a CO₂/CH₄ mixture selectivity differing from the ideal gas selectivity, suggesting non-Knudsen transport through the SWNT interior. In another work, Wu and Hinds¹⁶ have thoroughly mixed bulk nanotubes with epoxy resin and cut the cured CNT/epoxy composite into a 5- μ m-thick slice using a microtome. More recently, Mauter *et al.* have used a magnetic field to orient liquid crystal mesophases of hexagonally packed cylindrical micelles and to template the alignment of SWNTs sequestered in the micellar cores.¹²

Table 1 summarizes pros and cons of typical vertically aligned CNT (VACNT) membrane fabrication techniques. Unfortunately, all the CNT membranes produced so far suffer from at least one of the following drawbacks: 1) low density of CNT pores,^{17,18} 2) only partial CNT vertical alignment,¹⁸ 3) a brittle matrix,^{5,6} 4) rather small membrane active area and long fabrication processes,⁶ and 5) blocking of a large fraction of the pores by catalyst nanoparticles,¹⁷ excess matrix material,⁹ or polymerization inside the nanochannels.¹⁸ These issues have

hampered widespread successful production of CNT/polymer composite membranes that fully exploit the transport properties of the CNT channels. Hence, there still exists an impelling need for the development of defect-free, flexible, large active-area CNT membranes with well-aligned nanotubes and large pore density.

Choices of the polymeric matrix and specific processing steps are crucial for the successful fabrication of such CNT membranes. Liquid-phase processing such as the infiltration of a polymer solution into a CNT array often results in uneven CNT condensation, defects in polymer matrix, and loss of vertical CNT orientation during capillary condensation induced by solvent evaporation (Figure S1). One promising approach for controlling CNT alignment during the polymer composite fabrication is to infiltrate monomers into the pre-aligned nanotube array, followed by in-situ polymerization (Raravikar *et al.*¹⁹ and Huang *et al.*²⁰). By adopting this method here we overcome the typical limitation of polymer solution processes and demonstrate flexible, aligned-CNT/polymer composite membranes having relatively-high density CNTs. In our novel in-situ bulk polymerization method, end-protected vertically-aligned CNT arrays were infiltrated with styrene monomer with a certain amount of polystyrene-polybutadiene (PS-*b*-PB) block copolymer that acts as a plasticizer. A membrane matrix without larger structural defects obtained in this way combined high surface conformity with tunable flexibility. By adding PS-*b*-PB, the mechanical properties of the membrane were improved. Scanning electron microscopy (SEM) analysis also confirmed that alignment of CNTs remained undisturbed during the polymerization. These CNTs/polymer composite membranes showed very large gas and water permeabilities similar to those observed from the VACNT membranes reported in literatures,^{5,6,9,17,18,21} posing great promises in membrane applications that demand high flux, flexibility and durability.

2. Experimental Section

Membrane Fabrication

The procedure for CNT/polymer composite membrane fabrication is shown in Figure 1-(a). To maintain nanotube alignment during styrene monomer infiltration into CNT mats, a wet PVA (89% hydrolyzed, Sigma-Aldrich) film of *ca.* 500 μm in thickness was gently attached on the top of CNTs. The assembly was dried under a vacuum to remove any water in the PVA film. The assembled PVA/CNT array was placed between two glass slides with PTFE spacers and the mold was sealed using a 20wt% PVA solution as glue (Figure 1-(b)). The desired amount of PS-*b*-PB block copolymer (PS-*block*-PB-*block*-PS, styrene 30wt%, Mw \sim 140,000, Sigma-Aldrich) was dissolved in styrene monomer (Sigma-Aldrich) with magnetic stirring. After 10 hrs of mixing, 0.5 wt% of 2,2'-Azobisisobutyronitrile (Sigma-Aldrich) was added to the styrene monomer and PS-*b*-PB block copolymer mixture. The prepared mixture was injected into the mold and polymerized at 80 $^{\circ}\text{C}$ for 10 hrs in an argon-purged oven. Removal of the CNT/polymer composite from the mold could be easily achieved by dissolving PVA in warm water. The composite of polymer and CNT arrays was removed from silicon wafer with a 10 vol %

HF solution. A reactive ion etching (RIE) plasma (Samco, RIE-1C), using 4:1 ratio of CF_4/O_2 at 10 W power, was used to clean sample surfaces as well as to open the CNT ends (Figure 1-(c)).

In this study, performance of CNT/polymer composite membranes was compared directly to the performance of CNT/ SiN_x membranes under the same test condition. CNT/ SiN_x membranes were fabricated according to the previously reported method.⁶⁻⁸ Briefly, a VACNT array was grown on a silicon wafer coated with Fe/Mo catalyst *via* CVD using ethylene as the carbon precursor. Low pressure CVD of silicon nitride (SiN_x) filled the inter-nanotube gaps to form a membrane structure. Metallic nanoparticles on one side of the composite were removed by argon ion milling. RIE in oxygen-containing plasma removed the excess SiN_x layer on the other side of the composite and cut open the CNT end tips.

To grow VACNT arrays, we used a 1-inch quartz tube CVD furnace for the CNT/ SiN_x membrane fabrication, and a 4-inch wafer-scale, cold-wall furnace reactor (Black Magic, Aixtron) for the polymer/CNT composites membranes. Because of the different matrix infiltration method, we used VACNT mats with *ca.* 15-50 μm thickness for the CNT/polymer composite membrane fabrication, whereas 5- μm -thick CNT mats were used for the CNT/ SiN_x membrane. Average inner diameters of the VACNTs measured 3.3 nm and 1.6 nm⁶ for CNT/polymer composite and CNT/ SiN_x membranes, respectively.

Membrane Characterization

VACNT mats used for membrane fabrication were characterized by micro Raman (Nicolet Almega XR dispersive Raman spectrometer, Thermo Scientific) spectroscopy and high-resolution transmission electron microscopy (TEM). Gas permeance through the CNT membrane was measured using a constant pressure system equipped with a calibrated mass flow meter. Rejections of 5-nm-diameter colloidal Au nanoparticles (Ted-Pella), 0.5 mM potassium ferricyanide ($\text{K}_3\text{Fe}(\text{CN})_6$, Sigma-Aldrich) and methylene blue (Sigma-Aldrich) were evaluated by standard permeation tests using a custom-made, stainless-steel dead-end stirred cell designed for the CNT membrane test. The test cell was placed on a magnetic stir plate. The feed side was filled with 10 mL of test solution pressurized by nitrogen. The $\text{K}_3\text{Fe}(\text{CN})_6$ solutions collected at the permeate side of the CNT membranes were analyzed with UV-Vis spectroscopy (Shimadzu UV-Vis Spectrometer).

For the evaluation of mechanical properties of the composite membranes, we carried out an indentation test using a universal testing machine that we designed specifically for studies of ultralow-stiffness materials. Indentation was performed with a 1-mm-radius steel sphere (a precision ball bearing) attached to an XY manipulator stage bolted to a stepper motor (Compumotor 2100 series). The indenter displacement was measured with a micro encoder (Boeckeler Microcode encoder Model 1-845-X2) with a precision of 1 μm . As a load cell, we used an analytical microbalance (Mettler Toledo AT261, Delta range) to measure the force to a precision of 1 μN . The sample films were mounted on a cylinder with an inner diameter of 4.9 mm, using UV curable adhesive. The ball was centered onto the film with a precision of <50 μm and then indented at a rate of 100 $\mu\text{m}/\text{min}$.

3. Results and discussions

For a successful fabrication of CNT membranes several factors are of key importance: a) use of atomically smooth and well-graphitized CNTs; b) barrier properties of polymer matrix; c) easy exposure and opening of the CNT tips; d) achieving/maintaining vertical orientation of the CNTs while avoiding kinks/bends during fabrication; and e) mechanical stability of matrix.

a) *Quality of the CNT arrays*: Raman spectra (Figure 2-(b)) collected from the top of a 30- μm -thick VACNT forest (Figure 2-(a)) for polymer/CNT membrane fabrication indicate that the as-grown nanotubes are well-graphitized with a G (1595 cm^{-1})-to-D (1310 cm^{-1}) band ratio as high as 10 and with a clearly distinguished shoulder peak at 1560 cm^{-1} . Pronounced radial breathing mode suggests a large population of SWNTs and DWNTs. The TEM image shown in Figure 2-(c) clearly confirmed that the as-grown CNTs were SWNT or DWNT with low defect density. CNT inner diameter distribution was measured by analyzing about 30 samples in the TEM image. Figure 2-(d) shows that VACNT arrays with 30 μm thickness have a narrow diameter distribution from 2 to 5 nm with average 3.3 nm. Those used for CNT/SiN_x membrane fabrication were 1-to-2 nm wide. G/D ratio of the CNT arrays for the CNT/SiN_x membrane was close to 10 similar to that of CNT array for the polymer/CNT membrane.

b) *Barrier properties of polymer matrix*: As-synthesized CNT/polymer composite membrane before RIE etching didn't show any measurable gas flux through the membrane (detection limit $\sim 0.001\text{ sccm}$). In addition, we didn't see any liquid flux of as-synthesized composite film when using pressures up to 10 bar until the films were cracked at high feed pressure. Only a few minutes of RIE (typically 2- 5 min) was sufficient to open the pores of the composite membrane, allowing for preservation of the integrity of the PS/PS-b-PB matrix.

c) *Access and opening of the CNT tips*: A low and high magnification SEM image of the cross-section of the CNT composite (Figure 3-(a) and -(b)) clearly shows that, even before RIE etching, there is no excess polymer layer on the top of the composite film, and that most CNT end tips are protruding out of the composite surface.^{5,22} This absence of an excess layer is an important feature of our fabrication method for aligned CNT/polymer composite membranes. Most aligned CNT/polymer composites previously reported by other researchers had a relatively-thick excess polymer layer on the top of the CNT mats^{5,19} that needed to be removed by, for example, gentle mechanical polishing, plasma etching, or spin-coating using an organic solvent. These methods require long processing times and sometimes result in damages to the thin composite film. On the contrary, by minimizing any excess polymeric layer our technique requires only short and simple etching for exposing and opening the CNTs to permit fluid flow.

d) *CNT orientation*: To fully exploit CNT fast mass-transport properties in a membrane, it is also important to avoid bending or kinking of nanotubes in the polymer matrix during membrane fabrication. Figure 3-(c) shows a cross-sectional view of the sample after mild plasma etching to remove nanotubes that were pulled out of the array during the SEM sample preparation using liquid N₂. This high-magnification SEM image confirms that the CNTs remain well aligned in the polymer matrix.

e) Mechanical stability: Strong and flexible membrane films are desirable for any membrane applications. The mechanical properties of the CNT/polymer films were measured using a micro indentation method when PS or PS/PS-*b*-PB was used as a polymer matrix. It is difficult to measure modulus of the CNT/PS composite film because the CNT/PS samples are too stiff to calculate a modulus with the indentation method. Also, these samples are too brittle to be clamped in a sample loading cell of dynamic mechanical thermal analysis (DMTA) or Instron dynamic and fatigue system and therefore, elastic modulus of the CNT/PS sample is not discussed in this work. However, micro indentation measurements showed that the addition of 8 wt% PS-*b*-PB copolymer into the matrix improved the elongation at break of CNT/PS composite film by three times. Moreover, as shown in Figure 1-(c), the CNT/PS composite films prepared with addition of PS-*b*-PB copolymer as a plasticizer were flexible whereas CNT/PS composite films were quite brittle. The calculated elastic modulus of the CNT/PS/PS-*b*-PB membrane ranges between 470 and 980 MPa. It is lower than that of the wavy VACNT/epoxy composite (~ 5 GPa)²³ but higher than the modulus of VACNT/PDMS (~ 19 MPa)²⁴, porous PVDF (47-491 MPa)²⁵ and porous PTFE membrane (30 MPa) demonstrating its mechanical stability as membrane materials.²⁶

Our membrane characterization that included SEM imaging and measurement of fluid rates and selectivity for gas and liquid mixtures was consistent with having most of the flow going through nanometer-sized pores. Figure 3-(d) - a typical image of the surface of the composite film- shows CNTs embedded in a high-density polymer matrix free of large surface defects or pinholes. The quality of the membrane can also be characterized by measuring gas permeation dependence on the applied feed pressure. In general, gas transport through a porous membrane can be described by viscous flow, the Knudsen diffusion, and surface diffusion.²⁷ The Knudsen diffusion occurs when the mean free path of the gas molecules (λ) becomes larger than the membrane pore radius (r). In this condition, collisions of gas molecules with the pore walls are more dominant than molecule-molecule collisions. When r is larger than λ , as in the case for gas transport in pinholes or defects in membrane, intermolecular gas collisions in the viscous flow regime can dominate resulting in loss of gas selectivity. For porous membranes that are governed by Knudsen diffusion, the gas permeance in the Knudsen regime should be independent of the applied feed pressure, whereas it increases with pressure in the viscous regime. Figure 4-(a) shows the nitrogen permeability of CNT/polymer composite membrane at different feed pressures. Measured N₂ permeability through CNT membrane is independent of the applied feed pressures. This result means that there is no viscous flow through any large pinholes or large structural defects that is larger than λ of N₂ at room temperature, ~ 60 nm. In addition, following example of previous CNT membrane publications,⁶⁻⁸ we tested the prepared membranes for the filtration performance using analytes with small diameter. For these tests, we used 5-nm-diameter Au particles, 0.1 mM Direct Blue 71 (DB71), and 0.5 mM K₃Fe(CN)₆ solution (Figure 4-(b)–(d)). As shown in Figure 4-(b) and (c), permeating solution during filtration of 5 nm Au or DB71 solution through the membrane was clear suggesting complete rejection of the small analytes. In addition, UV-Vis spectroscopy analysis showed more than 90% salt rejection when a

0.5 mM $\text{K}_3\text{Fe}(\text{CN})_6$ solution was used for the filtration tests. As demonstrated previously, CNTs with negatively-charged carboxylate groups at their entrance exhibit significant ion exclusion for salts of multivalent anions and monovalent cations, even if the ion size is somewhat smaller than the CNT diameter.⁷ Here, DB71 has four negatively charged sulfonate groups on each monomer side, and its three-axes dimensions are about 3, 1.5, and 1 nm, respectively.²⁸ The reported hydrated radii of $\text{Fe}(\text{CN})_6^{3-}$ is around 0.475 nm.⁷ Although the average pore size of CNT used in this study is *ca.* 3 nm and ~10% of the CNTs are 4 nm wide, the presence of carboxylate groups at the CNT pore entrance explains the recorded high rejection for small negatively charged ions. These results also support that the prepared CNT/polymer composite membrane is free of larger defects or pinholes in polymer matrix.

For a successfully fabricated CNT/polymer membrane, we first compared gas and water permeabilities of the CNT/polymer membrane with the reference CNT/ SiN_x membrane. As shown in Figure 5, CH_4 , N_2 , and water permeabilities are all in narrow range, although there are differences in the exact magnitude of permeabilities. Calculated ideal selectivities of CH_4 over N_2 for CNT/polymer and CNT/ SiN_x are 1.48 and 1.51, respectively. These are higher than the Knudsen selectivity, 1.32, demonstrating that there is preferential interaction of hydrocarbons with CNTs side walls and that these two CNT membranes have similar gas transport properties. Water transport rates of two CNT membranes are similar although the average pore diameter of CNT array used in CNT/polymer fabrication is about twice that of CNT/ SiN_x membrane. Figure 6 shows the gas permeabilities of the CNT/polymer membrane as a function of the square root of the reciprocal of the molecular weight (*i.e.*, Knudsen model functional dependence on molecular mass) of several tested gases. The mechanism of gas transport through CNT in these conditions is still matter of debate. Previous and our experimental results in this work, however, show that for non-adsorbing gases such as He and N_2 gas transport scales with molecular weight as predicted by Knudsen theory.⁶ Since CNT membranes have much larger gas permeances than Knudsen model predictions, we scaled up the calculations of flow rates with Knudsen diffusion equation by a factor of 118 to match our experimental data. He and N_2 transport properties of the membrane agree well with the scaled Knudsen diffusion line. On the other hand, the CNT membranes showed higher selectivities for hydrocarbons and CO_2 than expected from the Knudsen scaling, suggesting preferential interaction of hydrocarbons and CO_2 with carbon nanotubes. These results are consistent with previously reported data for CNT membranes.^{6,9}

Following the analysis methods used in previous CNT membrane publications,⁶⁻⁸ we calculated enhancement factors for gas and water as well as corresponding slip lengths of the CNT/polymer membranes. Enhancement factors are shown in Figure 7. For comparison, we also plotted the enhancement factor and slip length of other CNT membranes,^{5,6,17,18,21,29} and theoretical estimations^{30,31} because we expect gas and water permeabilities in a range similar to that previously recorded for other CNT membranes, thus displaying analogous enhancement in the fluid transport rates with respect to Knudsen (gas) and Hagen-Poiseuille (water) theories. The accuracy for the calculation could be different for each of the CNT membranes described in the literature because of different fabrication process and different ways that the number of open

nanotubes was determined. While Hinds *et al.* estimated pore density of the MWNT membrane using KCl diffusion experiment,^{5,29} a nanotube density estimate of $2.0 \times 10^{11} \text{ cm}^{-2}$ of CNT/polymer membrane in this work was calculated with the weight-gain method.^{32,33} For CNT/SiN_x membrane, we used the estimate of $2.5 \times 10^{11} \text{ cm}^{-2}$ derived from the plan view TEM images of the membrane.⁶ Thus, our calculation for enhancement factor and slip length are lower boundary estimates because actual open number of nanotube for mass transport could be lower than our number estimated from weight-gain method and TEM images analysis. The SWNT membrane of Marand *et al.*,¹⁸ the MWNT membrane of Lin *et al.*,¹⁷ and the carbon pipes membrane of Quirke *et al.*²¹ estimated nanotube density using SEM images and we hypothesize their numbers are also lower boundary estimates similar to the pore density estimation in this work. Figure 7a shows calculated enhancement factors for gas. Because the mean free path of N₂ at room temperature ($\lambda \sim 60 \text{ nm}$) is significantly larger than the pore diameter of our membrane ($d = 3.3 \text{ nm}$), we have calculated the enhancement factor for N₂ based on the theoretical Knudsen model.

By assuming negligible contribution of surface flow of N₂ to the total flow, the gas flow rate can be expressed by the Knudsen equation:

$$J_{Kn} = \frac{2}{3} \sqrt{\frac{8\pi}{MRT}} \left(\frac{d}{2}\right)^3 V_m \frac{\Delta P}{L} \sigma A \quad (1)$$

where M is molecular weight, R is the universal gas constant, T is absolute temperature, d is pore diameter, V_m is the molar volume, ΔP is the pressure drop, L is the thickness of the membrane, σ is the areal DWNT density, and A is the test area of the membrane. The gas-flow enhancement is consistent with the atomistic simulations discussed above and the previous experimental observations of Hinds *et al.*^{5,29} and Holt *et al.*⁶ Interestingly, Figure 7a shows that N₂ enhancement factors of the CNT membranes prepared using CVD process and plasma etching process are similar although tube length/diameter, and the membrane fabrication methods are different. Although the CNT/PS membrane prepared by Lin *et al.*¹⁷ used the direct CVD growth of VACNT array, it shows lower enhancement factor possibly due to remained catalyst particles on the bottom of CNT tips embedded in polystyrene and alumina membrane support. The SWNT membrane prepared using post CNT alignment method also shows low enhancement factor similar to Lin *et al.*'s measurement.¹⁷ We hypothesize that the low value of the SWNT membrane is due to partial nanotube alignments and defects on the tube wall generated during the cutting process.

Following previous literature and extrapolating its validity to nanoscale, we used Hagen-Poiseuille equation with the inclusion of a slip-flow correction to estimate the volumetric flow rate Q_{SLIP} of water through long cylindrical pores:

$$Q_{SLIP} = \frac{\pi}{8\mu} \left[\left(\frac{d}{2} \right)^4 + 4L_s \left(\frac{d}{2} \right)^3 \right] \frac{\Delta P}{L}, \quad (2)$$

where μ is the water viscosity, and L_s is defined as the slip length:

$$L_s = \frac{U_{wall}}{dU/dr}, \quad (3)$$

where U_{wall} is the axial velocity at the wall, and dU/dr is the radial velocity gradient at the wall. In Figure 7b and c, we present the enhancement factor and slip length of CNT/polymer membrane for water. The results of CNT/polymer membrane are comparable to the CNT/SiN_x membrane.^{6,7} Contrary to the results of gas transport through CNTs, the values of the CNT/polymer membrane is lower than that of 1.6 nm diameter CNT/ SiN_x membrane and ~ 7 nm diameter MWNT/PS membrane. However, the CNT/polymer membrane shows higher enhancement factor than 43 nm carbon nanopipes membranes. Although there are uncertainties in estimation of areal nanotube density in each CNT membranes, the result suggests that the enhancement factor decreases with increasing tube diameter except the MWNT membrane by Hinds *et al.*^{5,29} In addition, these trends are consistent with molecular dynamics simulation studies, which suggest that the flow enhancement factor and slip length are dependent on CNT diameter.^{30,31} The water transport phenomena are more sensitive to nature of CNTs and the membrane fabrication method. Several molecular dynamics simulation studies have showed that the basic gas transport mechanism underlying the appearance of rapid diffusion in CNT pores is not strongly dependent on their diameter and length because gas molecules travel mostly near the CNT surface rather than moving ballistically across the pore.^{34,35} On the contrary, molecular dynamics simulation study for water transport through CNT suggested that slip length increases with decreasing CNT diameter because decreasing the CNT diameter weakens the coupling between water molecules and the carbon surface.³¹ This phenomenon induces curvature effects that influence the molecular density and distribution near the CNT wall. The curved surface pinches the low-energy potential wells and squeezes water molecules away from CNT surface, thus enhancing water flow rate and slip length. However, besides tube diameter, one should know that tube length and chirality could be other important parameters which can affect fluid transport through CNTs.

4. Conclusions

Flexible, robust and large-area membranes having VACNT arrays as pores were prepared by a novel in-situ polymerization method that prevents pore blocking and perturbation of nanotube alignment. Well-graphitized, vertical arrays of CNTs were infiltrated with a mixture of styrene monomer with a certain amount of polystyrene-polybutadiene (PS-b-PB) block copolymer that acts as a plasticizer. The VACNT/PS composite membrane with addition of PS-b-PB copolymer was flexible whereas VACNT/PS membrane was quite brittle. Microindentation measurements

confirmed that the addition PS-*b*-PB copolymer into the matrix improved the elongation at break of VACNT/PS film. SEM images showed that well aligned CNTs were embedded in a high-density polymer matrix free of any macroscopic voids or structural defects. Measured selectivity for gas and liquid mixtures using DB71, K₃Fe(CN)₆, or 5-nm Au particles also verified high quality of the CNT/polymer composite membrane. The gas and liquid transport properties of these VACNT/polymer composite membranes were comparable to that of other VACNT membranes reported in the literatures, demonstrating successful fabrication of flexible, VACNT/polymer composite membranes. These VACNTs/polymer membranes potentially enable applications that may require membranes with high flux, flexibility, and durability.

Acknowledgments

This work was partially supported by NSF NIRT CBET-0709090, DTRA (BB08PRO053 project) and DTRA (BA12PHM123) “Dynamic Multifunctional Materials for a Second Skin [D(MS)²] Focused Innovative Technology [FIT] Program”. Lawrence Livermore National Laboratory is operated by Lawrence Livermore National Security, LLC, for the U.S. Department of Energy, National Nuclear Security Administration under Contract DE-AC52-07NA27344. F. Fornasiero and S. Kim acknowledge support by DTRA-BB08PRO053 and DTRA-BA12PHM123. C. Grigoropoulos, O. Bakajin, and S. Kim acknowledge support by NSF NIRT CBET-0709090. H.G. Park acknowledges support by Swiss National Science Foundation (Contract Nr. 200021-137964).

References

- (1) Kong, J.; Franklin, N. R.; Zhou, C.; Chapline, M. G.; Peng, S.; Kyeongjae Cho; Dai, H. *Science* **2000**, 28, 622.
- (2) Collins, P. G.; Bradley, K.; Ishigami, M.; Zettl, A. *Science* **2000**, 287, 1801.
- (3) Calvert, P. *Nature* **1999**, 399, 210.
- (4) Planeix, J. M.; Coustel, N.; Coq, B.; Brotons, V.; Kumbhar, P. S.; Dutartre, R.; Geneste, P.; Bernier, P.; Ajayan, P. M. *J. Am. Chem. Soc.* **1999**, 116, 7935
- (5) Hinds, B. J.; Chopra, N.; Rantell, T.; Andrews, R.; Gavalas, V.; Bachas, L. G. *Science* **2003**, 303, 62
- (6) Holt, J. K.; Park, H. G.; Wang, Y.; Stadermann, M.; Artyukhin, A. B.; Grigoropoulos, C. P.; Noy, A.; Bakajin, O. *Science* **2006**, 312, 1034
- (7) Fornasiero, F.; Park, H. G.; Holt, J. K.; Stadermann, M.; Grigoropoulos, C. P.; Noy, A.; Bakajin, O. *Proceedings of the National Academy of Sciences of the United States of America* **2008**, 105, 17250.
- (8) Fornasiero, F.; Bin In, J.; Kim, S.; Park, H. G.; Wang, Y.; Grigoropoulos, C. P.; Noy, A.; Bakajin, O. *Langmuir* **2010**, 26, 14848.
- (9) Kim, S.; Jinschek, J. R.; Chen, H.; Sholl, D. S.; Marand, E. *Nano Lett.* **2007**, 7, 2806.
- (10) Mi, W.; Lin, Y. S.; Li, Y. *Journal of Membrane Science* **2007**, 304, 1.
- (11) Yu, M.; Funke, H. H.; Falconer, J. L.; Noble, R. D. *Nano Letters* **2009**, 9, 225.
- (12) Mauter, M. S.; Elimelech, M.; Osuji, C. O. *Acs Nano* **2010**, 4, 6651.
- (13) Hummer, G.; Rasaiah, J. C.; Noworyta, J. P. *Nature* **2001**, 414, 188.
- (14) Skoulidas, A. I.; Ackerman, D. M.; Johnson, J. K.; Sholl, D. S. *Physical Review Letters* **2002**, 89, 185901.
- (15) Majumder, M.; Chopra, N.; Andrews, R.; Hinds, B. J. *Nature* **2005**, 438, 44.
- (16) Wu, J.; Paudel, K. S.; Strasinger, C.; Hammell, D.; Stinchcomb, A. L.; Hinds, B. J. *Proceedings of the National Academy of Sciences of the United States of America* **2010**, 107, 11698.
- (17) Mi, W.; Lin, Y. S.; Li, Y. *Journal of Membrane Science* **2007**, 304, 1.
- (18) Surapathi, A.; Herrera-Alonso, J.; Rabie, F.; Martin, S.; Marand, E. *Journal of Membrane Science* **2011**, 375, 150.
- (19) Raravikar, N. R.; Schadler, L. S.; Vijayaraghavan, A.; Zhao, Y. P.; Wei, B. Q.; Ajayan, P. M. *Chemistry of Materials* **2005**, 17, 974.
- (20) Huang, H.; Liu, C. H.; Wu, Y.; Fan, S. S. *Advanced Materials* **2005**, 17, 1652.
- (21) Whitby, M.; Cagnon, L.; Thanou, M.; Quirke, N. *Nano Letters* **2008**, 8, 2632.
- (22) Kang, M.; Myung, S. J.; Jin, H. J. *Polymer* **2006**, 47, 3961.
- (23) Cebeci, H.; Villoria, R. G. d.; Hart, A. J.; Wardle, B. L. *Composites Science and Technology* **2009**, 69, 2649.
- (24) Ci, L.; Suhr, J.; Pushparaj, V.; Zhang, X.; Ajayan, P. M. *Nano Letters* **2008**, 7, 2762.
- (25) Feng, C.; Shi, B.; Li, G.; Wu, Y. *Journal of Membrane Science* **2004**, 237, 15.
- (26) Ko, W.-C.; Tseng, C.-K.; Wu, W.-J.; Lee, C.-K. *E-Polymers* **2010**, 32.
- (27) Uhlhorn, R. J. R.; Keizer, K.; Burggraaf, A. J. *Journal of Membrane Science* **1989**, 46, 225.
- (28) Ren, T.-Z.; Yuan, Z.-Y.; Su, B.-L. *Colloids and Surfaces a-Physicochemical and Engineering Aspects* **2007**, 300, 79.
- (29) Majumder, M.; Chopra, N.; Hinds, B. J. *Acs Nano* **2011**, 5, 3867.
- (30) Thomas, J. A.; McGaughey, A. J. H. *Nano Letters* **2008**, 8, 2788.
- (31) Thomas, J. A.; McGaughey, A. J. H. *Physical Review Letters* **2009**, 102.
- (32) Zhong, G.; Warner, J. H.; Fouquet, M.; Robertson, A. W.; Chen, B.; Robertson, J. *Acs Nano* **2012**, 6, 2893.

- (33) Esconjauregui, S.; Xie, R.; Fouquet, M.; Cartwright, R.; Hardeman, D.; Yang, J.; Robertson, J. *Journal of Applied Physics* **2013**, *113*.
- (34) Skoulidas, A. I.; Sholl, D. S.; Johnson, J. K. *Journal of Chemical Physics* **2006**, *124*, 054708/1.
- (35) Chen, H.; Johnson, J. K.; Sholl, D. S. *J. Phys. Chem. B* **2006**, *110*, 1971.

Table 1. Typical vertically aligned CNT membrane techniques reported in the literatures

CNT	Pore diameter (nm)	Matrix/fabrication method	Density ($\times 10^{10} \text{ cm}^{-1}$)	Advantages	Disadvantages
Post aligned SWNT ¹⁸	1.2	Polyacrylate copolymer/in-situ polymerization	0.7	• Scalability	• Low CNT density • Partial CNT alignment • Possible CNT damage during cutting process
CVD-DWNT ⁶	1.6	SiNx/CVD	25	• Fast flux • High enhanced flow	• Complicated membrane fabrication process • Poor mechanical properties
CVD-MWNT ¹⁷	6.3	Polystyrene/solution casting	0.19	• Scalability/simple process	• Low CNT density • Low flux
CVD-MWNT ⁵	7.0	Polystyrene/solution casting	6	• Fast flux • High enhanced flow	• Poor mechanical properties
Carbon deposition ²¹	43	CVD deposition of carbon on Anodic aluminum oxide	1.07	• Simple process	• Poor mechanical properties • Low flux enhancement

Figure index

Figure 1. (a) Fabrication procedure. Step 1: attachment of PVA film on CNT array; 2: in-situ polymerization; 3: PVA film and Si-wafer removal; 4: RIE etching. (b) polymer solution injection into the mold. (c) prepared CNT/polymer composite sample.

Figure 2. Characterization of CNT arrays: (a) SEM images of vertically aligned CNT array with 30 μm thickness, (b) Raman spectra for the full $100\text{--}3400\text{ cm}^{-1}$ range, (c) a representative TEM image used to determine the CNT diameter distribution, and (d) inner diameter distribution of CNTs determined from (c).

Figure 3. SEM images (a) lower magnification (b) higher magnification showing no excess polymer layer on the top of CNT composites (c) higher magnification after plasma etching showing aligned CNTs in polymer matrix and (d) higher magnification of top surface of CNT/polymer membrane.

Figure 4. (a) N_2 permeability at different feed pressure, (b) 5 nm Aucolloid filtration test, (c) 0.1 mM DB71 exclusion test, and (d) 0.5 mM K_4FeCN_6 exclusion test.

Figure 5. Gas and water permeabilities of CNT/polymer and CNT/SiN_x membranes.

Figure 6. Single-gas permeability as a function of the inverse square root of the molecular weight of the penetrant.

Figure 7. Calculated (a) enhancement over Knudsen model, (b) enhancement over no-slip, hydrodynamic model, and (c) slip length.

Figure 1. (a) Fabrication procedure. Step 1: attachment of PVA film on CNT array; 2: in-situ polymerization; 3: PVA film and Si-wafer removal; 4: RIE etching. (b) polymer solution injection into the mold. (c) prepared CNT/polymer composite sample

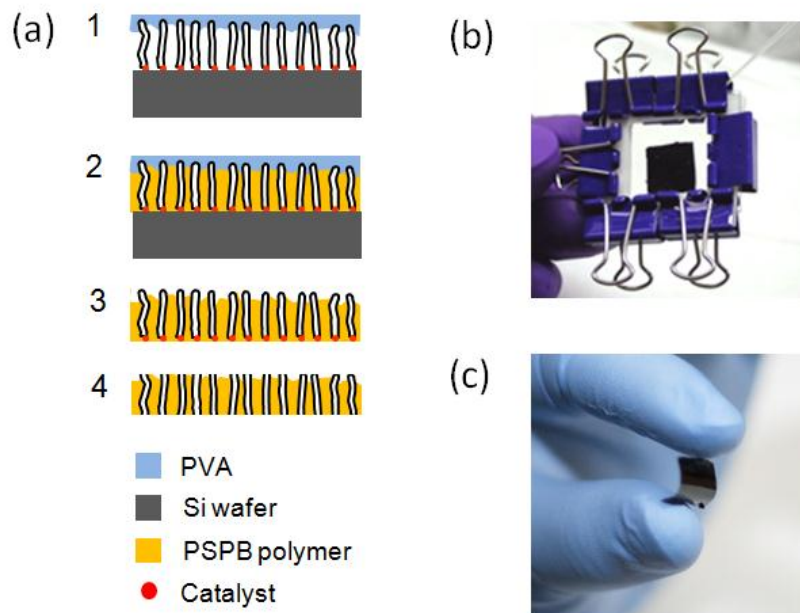


Figure 2. Characterization of CNT arrays: (a) SEM images of vertically aligned CNT array with 30 μm thickness, (b) Raman spectra for the full 100–3400 cm^{-1} range, (c) a representative TEM image used to determine the CNT diameter distribution, and (d) inner diameter distribution of CNTs determined from (c).

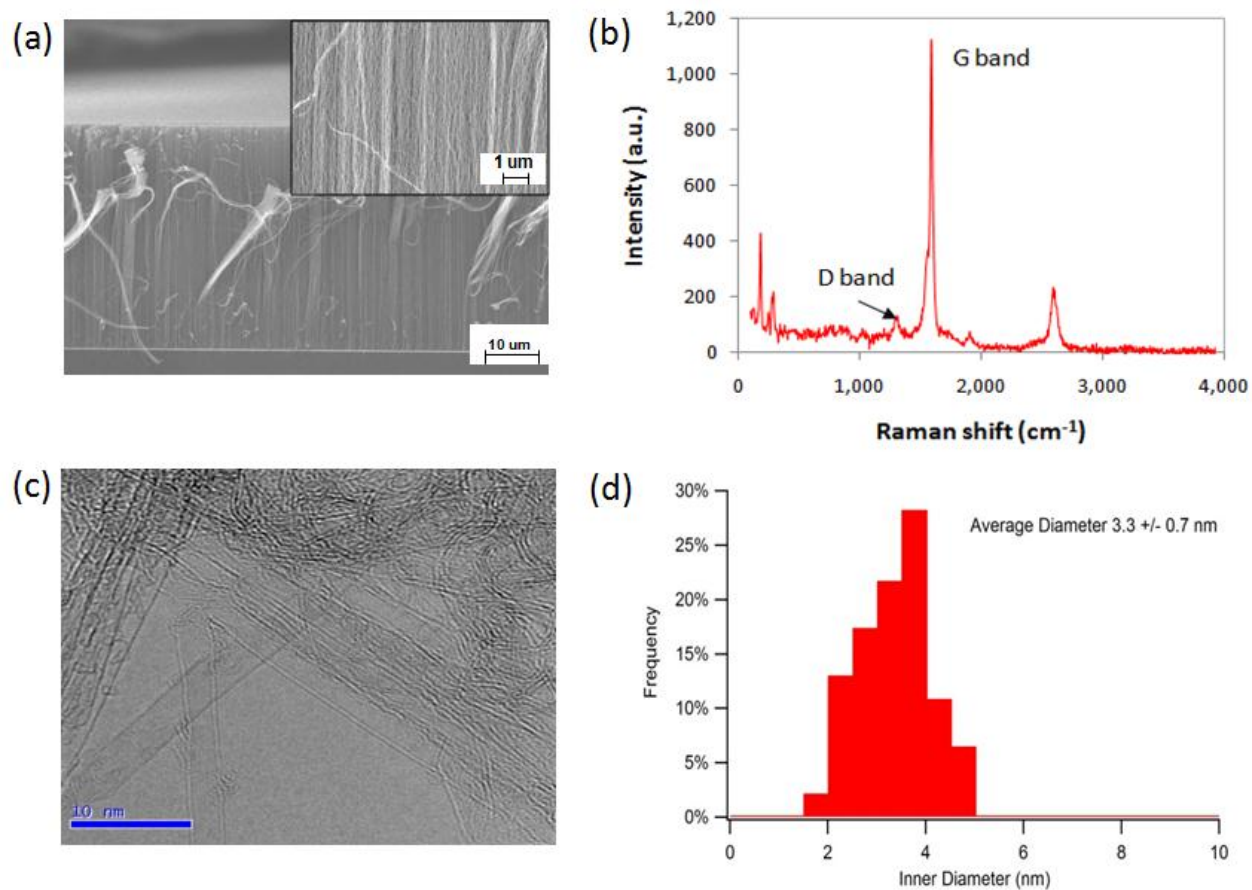


Figure 3. SEM images (a) lower magnification (b) higher magnification showing no excess polymer layer on the top of CNT composites (c) higher magnification after plasma etching showing aligned CNTs in polymer matrix, and (d) higher magnification of top surface of CNT/polymer membrane.

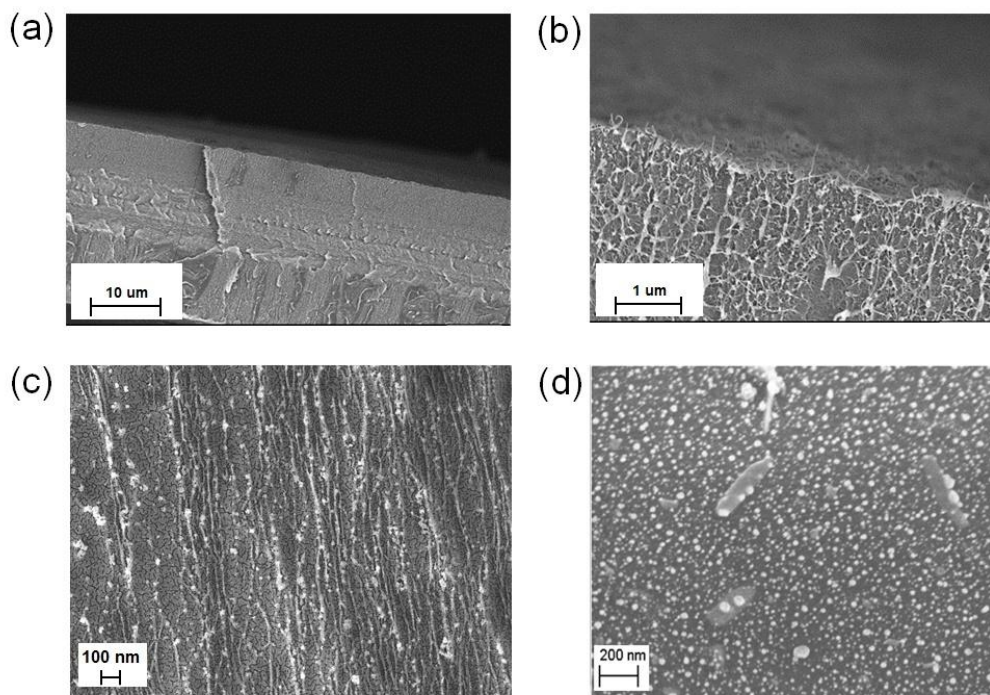


Figure 4. (a) Nitrogen permeability at different feed pressures, (b) 5 nm goldcolloid filtration test, (c) 0.1 mM DB71 exclusion test, and (d) 0.5 mM potassium ferricyanide exclusion test.

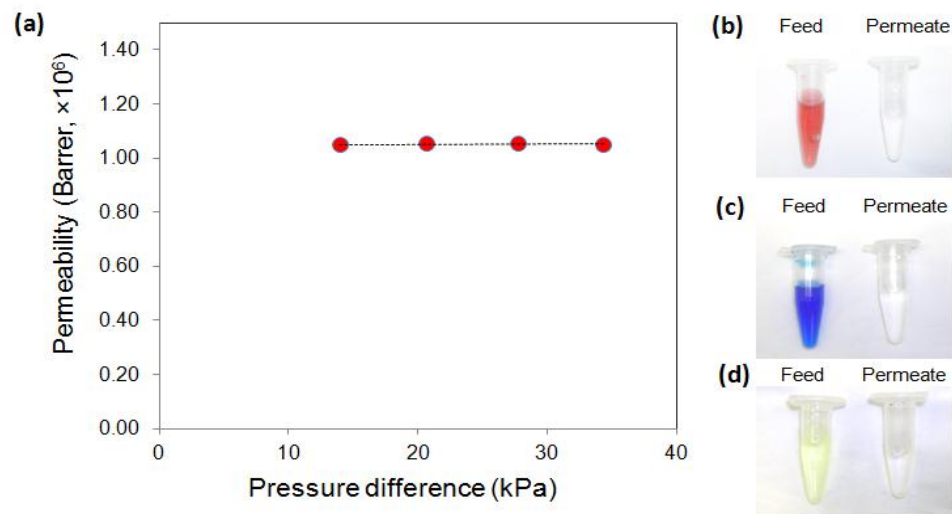


Figure 5. Gas and water permeabilities of CNT/polymer and CNT/SiN_x membranes.

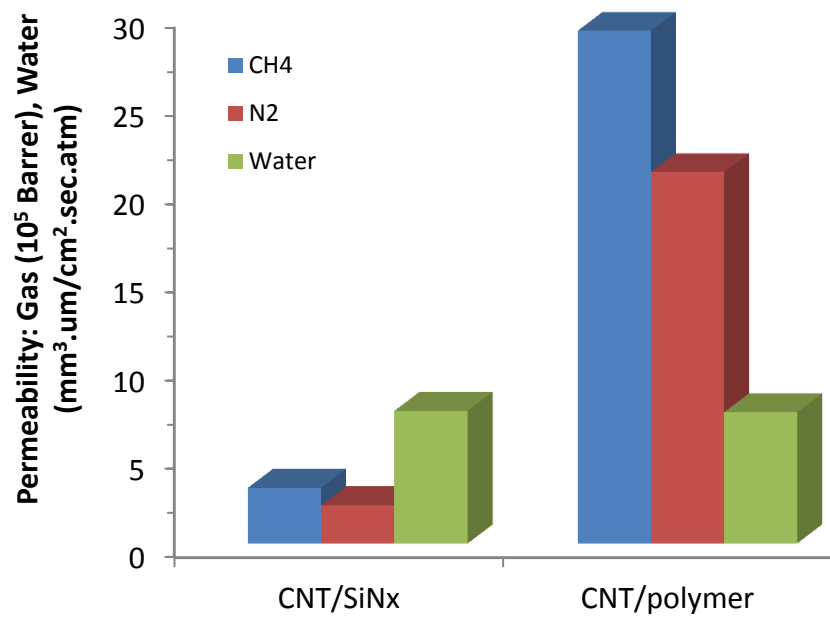


Figure 6. Single-gas permeability as a function of the inverse square root of the molecular weight of the penetrant.

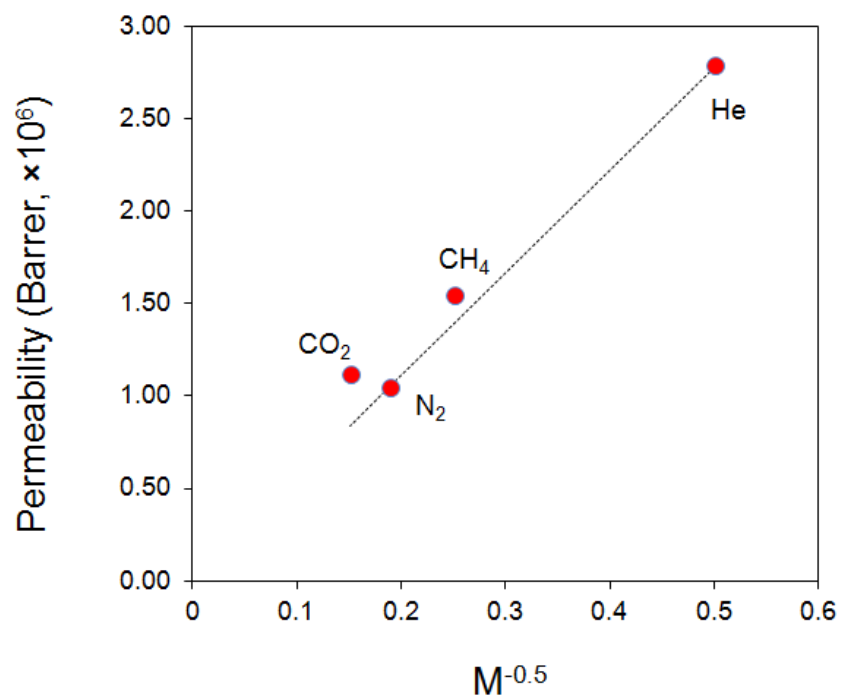
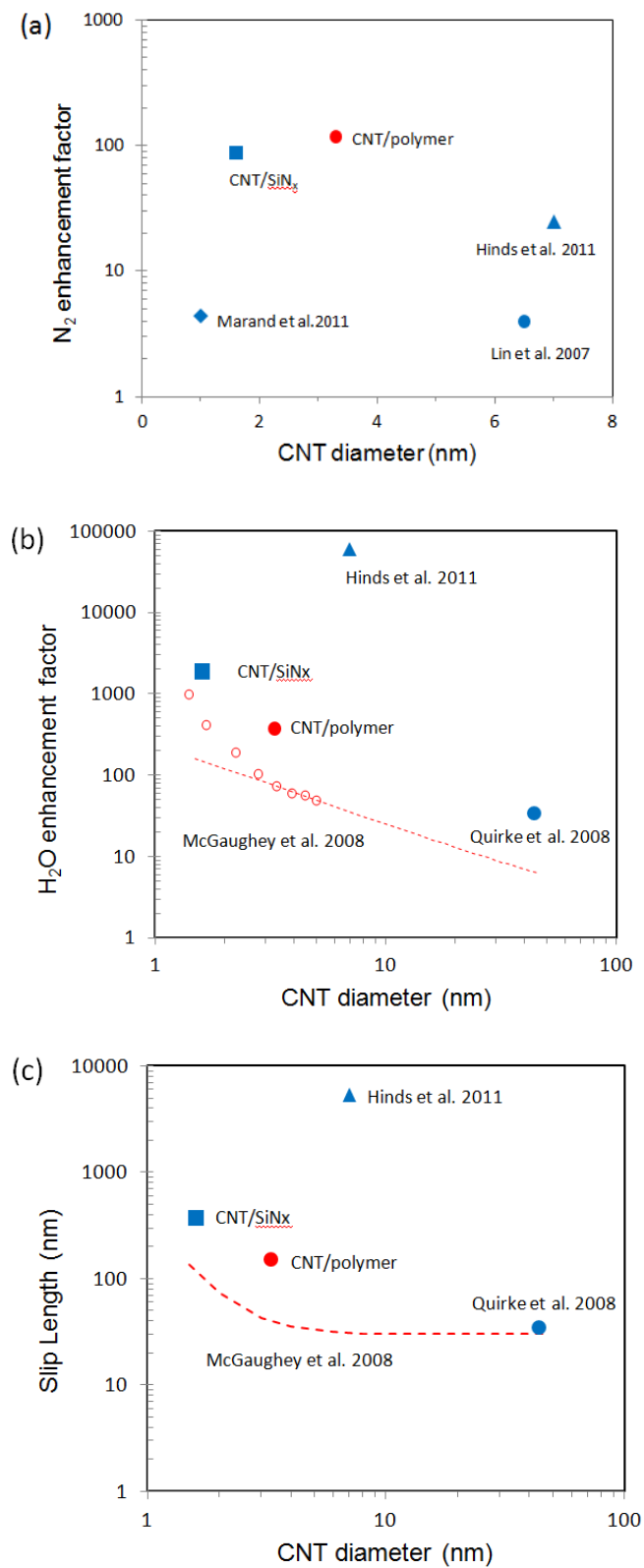


Figure 7. Calculated (a) enhancement over Knudsen model, (b) enhancement over no-slip, hydrodynamic model, and (c) slip length.



Supporting Information

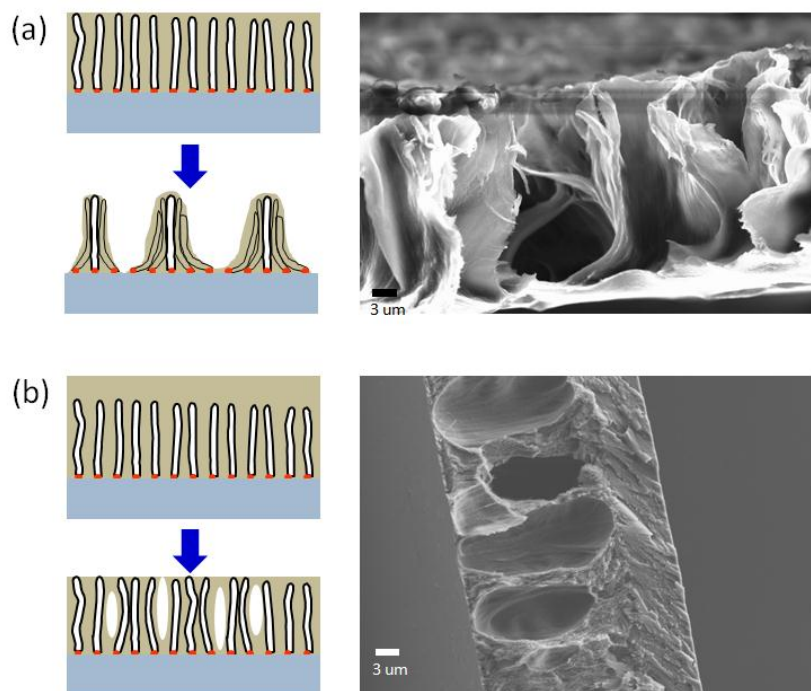


Figure S1. SEM images of CNT/polymer composites prepared with polymer solution casting method. (a) CNT condensation and (b) voids in composite.